High-efficiency generation of circularly polarized light via symmetry-induced anomalous reflection

Shang-Chi Jiang, Xiang Xiong, Yuan-Sheng Hu, Sheng-Wei Jiang, Yu-Hui Hu, Di-Hu Xu, Ru-Wen Peng,[*] and Mu Wang[†]

National Laboratory of Solid State Microstructures, School of Physics, and Collaborative Innovation Center of Advanced Microstructures, Nanjing University, Nanjing 210093, China

Great efforts have been devoted to control the polarization state, the transmission direction, and the phase of light within a very confined space in recent decades. Here, we present a two-dimensional metastructure made of an array of unisized split rings with different opening orientations on the surface of a SiO_2-silver bilayer. This structure possesses an unexpectedly high polarization conversion ratio and generates significantly strong anomalous reflection beams (over 70% of incident light intensity) over a broad frequency range (1100–1750 nm). Functionally, it is able to turn either a linearly polarized incident light or natural light into two perfect circularly polarized beams with the same amplitude yet different handedness to different directions. These features demonstrate a clear example of momentum conservation and can be applied to detect/manipulate the propagation of circularly polarized light.

PACS number(s): 78.67.Pt, 42.25.Ja, 42.25.Bs

Manipulating the spin state of electrons is an important process in quantum information technology, and it can be realized by using circularly polarized light [1–4]. However, on a nanometer scale, generation, sorting, and detection of circularly polarized light remains an underdeveloped area in photonics [5,6]. Despite that the concept of "metasurface" has made a big step forward in controlling the polarization of light [7,8], the narrow bandwidth and weak intensity of the circularly polarized light generated by the metasurface [9,10] seriously limit its applications. Traditionally, in order to generate circularly polarized light, a combination of a linear polarizer and a quarter wave plate is applied [11,12]. However, the wave plate is usually made of birefringence crystal with certain thickness and noticeable dispersion; hence, it becomes inapplicable beyond a certain frequency range.

In the past two decades, people have found that closely stacked metallic nanostructures can effectively tune the polarization state of light [13–21]. An assembly of two-dimensional subwavelength metallic structures, known as a metasurface [7,8,22,23], can effectively manipulate the ray trajectories [24–32] and the polarization state of light [10,21,33], generate a vortex beam [34,35], and convert propagating waves into surface waves [9,36]. The gradient of phase discontinuity on the metasurface may induce a refraction beam, which does not obey conventional Snell's law and propagates in a specific trajectory [7,37,38]. This beam is hence termed as the anomalous beam. The gradient of phase discontinuity on the metasurface depends on the shape, size, and orientation of each individual building block. For example, in Ref. [33], the metasurface is constructed by two groups of geometrically offset V shapes with different opening angles. The polarization of the anomalous beam is controlled by the offset of the subunits. Another example is that, by assembling identical straight gold nanorods pointing to different orientations on a substrate surface, a left-hand circularly polarized (LCP) transmission beam and a right-hand circularly polarized (RCP) transmission beam are generated and propagate separately in different directions [10,30].

In Refs. [10,30], the phase of the reflected or transmitted circularly polarized light is determined by rotating the unit cell, which is termed as the Pancharatnam-Berry phase [39–41]. The Pancharatnam-Berry phase ensures the existence of the circularly polarized anomalous beam, yet improving the beam intensity remains an important issue for a metallic metasurface.

In addition to intensity, the bandwidth is another important issue in the application of a metasurface. Upon illumination of incident light, free electrons on the surface of a metallic structure can be excited, forming oscillating surface electric current. The electromagnetic field adjacent to the metallic structure can be modulated by irradiation of the oscillating surface electric current. At the resonance frequency, this effect is so significant that a thin layer of metallic structure can effectively tune the polarization state of light. However, the Lorentz resonance in metal is highly dispersive, which makes this effect evident only in a very narrow frequency range. In contrast, dielectric material interacts with light by accumulating an optical path in space. This feature exists over a broad bandwidth and has already been applied for antireflective coating and many other optical devices [11,42]. Combining a metallic metastructure and dielectric interlayer makes the dispersion-free broadband device possible, where the strong response of the metallic structures helps to miniaturize the device, and the dielectric interlayer helps to eliminate the dispersion simultaneously in both amplitude and phase difference of the reflected/transmitted light [21,43,44]. Specifically, it has been recently demonstrated [21] that, by introducing a compact metallic reflecting layer underneath the metallic metastructures and the dielectric interlayer, a conjugation system is constructed. By properly selecting the structural parameters, the intrinsic dispersion of the metallic structures can be perfectly cancelled out by the thickness-dependent dispersion of the dielectric spacing layer [21].

When a linearly polarized light is reflected on an anisotropic structure, the polarization of the reflected light can be partly changed from its original direction to the orthogonal direction. This phenomenon is known as the polarization conversion effect [41,45]. The ratio of the intensity of the cross-polarized reflected light and that of the incident light is defined as the polarization conversion ratio. This ratio has been found to

―――――――
*rwpeng@nju.edu.cn
†muwang@nju.edu.cn

play an important role in enhancing the linearly polarized anomalous beam [43,46].

In this paper, we demonstrate a metasurface made of an array of split ring resonators with the identical geometrical size yet different opening orientations. The array of split rings is fabricated on top of a SiO$_2$-silver bilayer. By rotating the split ring to different orientations on the metasurface, according to Refs. [10,39–41], a Pancharatnam-Berry phase is generated. It follows that LCP and RCP anomalous beams are consequently generated. We theoretically prove that the light intensity of the anomalous beam is determined by the polarization conversion ratio of the building blocks (the split rings). By constructing a unit cell with 16 split rings with rotating orientations, we experimentally show that this metasurface is able to convert more than 70% of incidence energy to the anomalous reflection beam in the range of 1100–1750 nm. Further, LCP and RCP beams can be effectively generated with either linearly polarized incident light or natural light. For circularly polarized incidence, the propagation direction of the LCP/RCP beam is changed, whereas their original handedness resumes.

The building block of our metasurface is designed as a silver split ring sitting on top of the SiO$_2$-silver bilayer substrate, with its opening pointing in the 45° direction, as illustrated in Fig. 1(a). The inner radius of the ring r is designed as 127.5 nm. The thickness d and width b of the split ring are 50 and 70 nm, respectively. The thickness of the SiO$_2$ layer h_1 and that of the silver layer h_2 are 175 and 100 nm, respectively. The separation of the building block is set as 600 nm. The coordinate system u-v-w is set on the split ring, which changes its orientation when the split ring is rotated. Due to the existence of the reflection silver layer underneath the split ring array, the transmission of the structure is zero. The finite difference time domain (FDTD) method is applied to calculate the reflection of the structure, and a

sample consisting of identical split rings (both geometrical size and orientation) is fabricated to measure the reflectance of the building block experimentally. The simulated and exactly measured reflectance of the array are illustrated in Fig. 1(b), where r_{ij} represents the normalized complex amplitude of the i component of the reflected light corresponding to j polarized incidence ($i,j = u,v$). It is noteworthy that for v-polarized incidence, the symmetry axis of the building block is along 45° [Fig. 1(a)], the reflected light contains both u-polarized and v-polarized components. This means that the polarization conversion does occur in this scenario. This effect is quantitatively expressed by the polarization conversion ratio $|r_{uv}|^2$. By tuning the thickness of the silicon dioxide layer between the split ring array and the reflection silver layer, the dispersion of the reflection spectrum can be manipulated [21]. Therefore, a large polarization conversion ratio can be realized in a broad wavelength range. As illustrated in Fig. 1(b), the surface possesses a high polarization conversion ratio for the wavelength between 1100–1750 nm. This means that the u component of the reflected light can be effectively excited by the v component of the incident light. Since the symmetry axis is in 45°, the v component of the reflected light can also be excited by the u-polarized incident light as well. It follows that $r_{uu} = r_{vv}$ and $r_{vu} = r_{uv}$. In Fig. 1(b), despite that the measured $|r_{uv}|^2$ is slightly smaller than the simulation due to the imperfection in sample fabrication, the experimental measurement is in good agreement with the simulation.

A high polarization conversion ratio is essential to enlarge the amplitude of the anomalous beam. When the orientation of the opening of each split ring rotates on the surface of the substrate, a rotation-induced phase gradient is generated. As a result, the anomalous beams with LCP/RCP features appear. To express the light intensity of the anomalous beams, two coordinate systems are applied to calculate the reflection from the building block, as illustrated in Fig. 1(c). The x-y-z axes remain in the original orientations, whereas the u-v-w axes locate on the split ring building block and rotate together with the split ring. The split ring is rotated anticlockwise with respect to its own center by an angle φ, which equals the angle between the u and x axes. The reflection of the structure in the u-v-w coordinate system is already calculated, as shown in Fig. 1(b). When incident light shines on the structure, we can first decompose the incidence to u and v axes and then calculate the reflection in the u-v-w coordinate system. For y-polarized incidence, the normalized electric component is expressed as $\hat{e}_y$. In the u-v coordinate system, the y-polarized electric component is expressed as the superposition of $\cos\varphi\hat{e}_v$ and $\sin\varphi\hat{e}_u$, as that shown by the green arrows in Fig. 1(c), and $\hat{e}_y$, $\hat{e}_v$, and $\hat{e}_u$ are the unit vectors in the y, v, and u axes, respectively. The electric component of the reflected light excited by $\sin\varphi\hat{e}_u$ and $\cos\varphi\hat{e}_v$ is expressed as $\vec{E}_{1y}$ and $\vec{E}_{2y}$,

$$\vec{E}_{1y} = \sin\varphi r_{uv}\hat{e}_v + \sin\varphi r_{vv}\hat{e}_u,$$
$$\vec{E}_{2y} = \cos\varphi r_{vv}\hat{e}_v + \cos\varphi r_{uv}\hat{e}_u. \tag{1}$$

We can now regroup the four terms in $\vec{E}_{1y}$ and $\vec{E}_{2y}$ into two linearly polarized components $\vec{E}_{ry}$ and $\vec{E}_{sy}$ as

$$\vec{E}_{ry} = \sin\varphi r_{uv}\hat{e}_v + \cos\varphi r_{uv}\hat{e}_u = r_{uv}\hat{e}_{ry},$$
$$\vec{E}_{sy} = \cos\varphi r_{vv}\hat{e}_v + \sin\varphi r_{vv}\hat{e}_u = r_{vv}\hat{e}_{sy}. \tag{2}$$
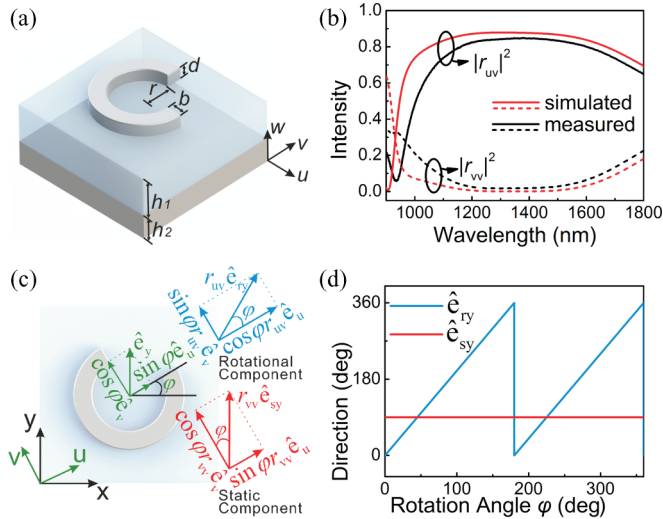
FIG. 1. (Color online) (a) The split ring building block of the metasurface. (b) The simulated and measured reflectance of the array of the building blocks. (c) The schematic of the light reflected by the building block rotated with an angle φ. The rotational and static components are marked by blue and red arrows, respectively. (d) The plot to show the polarization direction of the two components of reflected light as a function of the rotation angle φ.

Here, the subscript y in $\vec{E}_{ry}$ and $\vec{E}_{sy}$ indicates that the incident light is y polarized, $\hat{e}_{ry}$ and $\hat{e}_{sy}$ express the unit vectors of $\vec{E}_{ry}$ and $\vec{E}_{sy}$, respectively. $\vec{E}_{ry}$ and $\vec{E}_{sy}$ are illustrated, respectively, by the blue and red arrows in Fig. 1(c). The relation between angle φ and the direction of the rotational and the static components $\hat{e}_{ry}$ and $\hat{e}_{sy}$ is illustrated in Fig. 1(d). One may find that the direction of $\hat{e}_{ry}$ is pointing to 2φ (the blue line); while $\hat{e}_{sy}$ remains pointing in the $+y$ direction (90°, the red line), which is the same as that of the incident light. By rotating the building block, $\hat{e}_{ry}$ rotates accordingly, so we denote $\vec{E}_{ry}$ as the *rotational component*. In contrast, $\hat{e}_{sy}$ does not change orientation when the building block is rotated, so we denote $\vec{E}_{sy}$ as the *static component*. The reflected light under y-polarized incidence $\vec{r}_{\text{ref},y}$ can be expressed as the superposition of $\vec{E}_{ry}$ and $\vec{E}_{sy}$. It follows that

$$\vec{r}_{\text{ref},y} = r_{vv}\hat{e}_{sy} + r_{uv}\hat{e}_{ry}. \tag{3}$$

Equation (3) represents the reflection from a certain building block with rotation angle φ, which can be applied to retrieve the physical properties of the metasurface.

As illustrated in Fig. 2(a), the unit cell of our metasurface is constructed by a queue of 16 split rings with the identical geometrical size but different opening orientations, where the opening of each split ring has been rotated anticlockwise by $\Delta\varphi = 22.5°$ with respect to the neighboring one. The metasurface is constructed by reproducing the unit cell in both x and y directions in the plane. The generalized Snell's law [7] is applied to describe the direction of the reflection beam from the metasurface. In our design, the phase of the reflected light changes only in the x direction. For normal incidence, the reflection direction is expressed as

$$\sin\theta = \frac{\lambda_0}{2\pi}\frac{d\Phi}{dx}, \tag{4}$$

where θ is the reflection angle, λ_0 is the wavelength, and $\frac{d\Phi}{dx}$ is the phase gradient of the reflected light, respectively. For nonzero $\frac{d\Phi}{dx}$, the reflection angle does not equal the incident angle, which is counterintuitive. Hence, this reflected light is termed as the anomalous beam. If the phase gradient $\frac{d\Phi}{dx}$ vanishes on the metasurface, the reflection beam obeys the conventional Snell's law.

The phase gradient on the metasurface can be calculated by analyzing the direction of rotational and static components of each ring in a unit cell. For the scenario of y-polarized normal incidence [marked as $\vec{E}_{\text{in}}$ in Fig. 2(a)], within each unit cell, the polarization directions of the rotational and static components corresponding to each individual split ring are illustrated in Fig. 2(a). The superposition of the rotational and static components reflected by the structure generates the reflected light. For the static components, the amplitude, the propagation direction, and the phase do not depend on the rotation of the ring, so the phase gradient is zero. According to Eq. (4), zero phase gradient means that the reflected light obeys the conventional Snell's law. For normal incidence, the reflection angle is 0 (i.e., along the $+z$ direction). The intensity of the ordinary beam is determined by the amplitude of the static component reflected by each split ring $|r_{vv}|$. Since the static component is y polarized, it follows that the ordinary beam is y polarized as well with intensity $|r_{vv}|^2$.
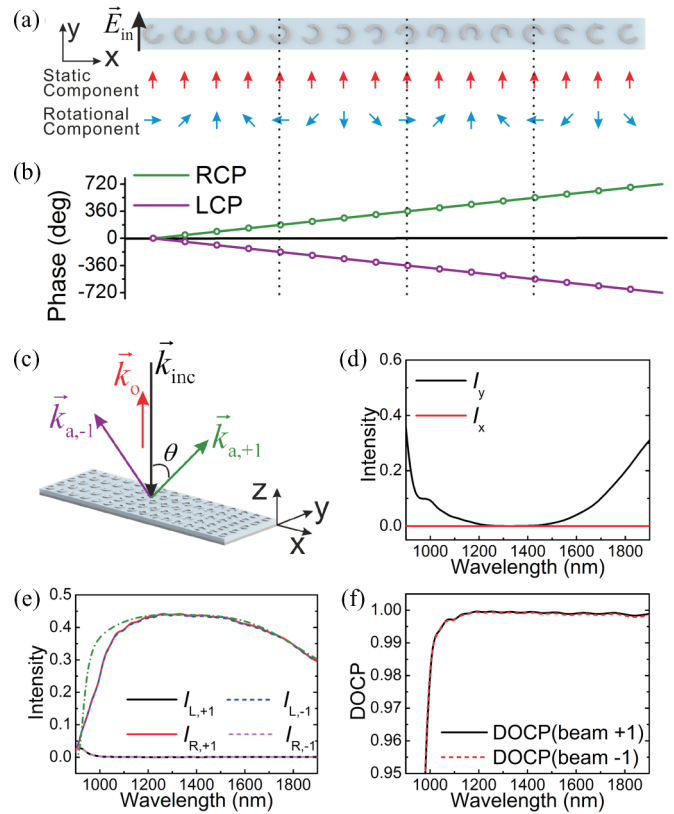
FIG. 2. (Color online) (a) The unit cell of the metasurface. The red and blue arrows correspond to the polarization direction of the static and rotational components reflected by each building block, respectively. $\vec{E}_{\text{in}}$ represents the polarization of the incident light. (b) The phase of the RCP and LCP components of the rotational component shown in (a). (c) The schematic shows the direction of incident light and reflected light. $\vec{k}_{\text{inc}}$, $\vec{k}_o$, $\vec{k}_{a,+1}$, and $\vec{k}_{a,-1}$ are the wave vectors of incident light, ordinary beam, anomalous beams $+1$ and -1, respectively. (d) The simulated intensity of x and y components of the ordinary beam. (e) The intensity of LCP and RCP components of anomalous beams. The green dashed-dotted line denotes $|r_{uv}|^2/2$. (f) The DOCP of the anomalous beam $+1$ and -1 as a function of wavelength.

A linearly polarized light can be treated as the superposition of circularly polarized beams with the same amplitude yet different handedness, i.e., with both LCP and RCP beams. Since the rotational component reflected by each split ring is linearly polarized, it can be represented by a LCP and RCP component. The phases of LCP and RCP components are illustrated with the purple and green lines in Fig. 2(b), respectively. The phase gradient $d\Phi/dx$ of the RCP component is $\pi/4l$, and that for the LCP component possesses the same value but opposite sign. Since the amplitude of the rotational component is $|r_{uv}|$, the total intensity of the anomalous beams is therefore $|r_{uv}|^2$. It follows that the intensity of each LCP and RCP anomalous beam is $|r_{uv}|^2/2$, respectively. The reflection angle of LCP and RCP beams can be calculated based on Eq. (4). Figure 2(c) schematically illustrates the propagation of the anomalous beam and ordinary beam. For the y-polarized normal incidence (marked as $\vec{k}_{\text{inc}}$), the propagation direction of the ordinary beam $\vec{k}_o$ remains along the z axis, which is

marked by the red arrow in Fig. 2(c). Two anomalous beams, located on the two sides of the z axis and marked as anomalous beam $+1$ ($\vec{k}_{a,+1}$) and -1($\vec{k}_{a,-1}$), correspond to RCP and LCP components, respectively, shown in Fig. 2(b).

The reflection spectra of the ordinary and anomalous beams are calculated in Figs. 2(d) and 2(e). Figure 2(d) demonstrates the intensity of x and y components of the ordinary beam when the incidence is y polarized. In the wavelength range of 1100–1750 nm, the x component vanishes [Fig. 2(d)]. Therefore, the reflected light is y polarized. The spectrum of the y component of the ordinary beam in the response wavelength range is almost the same as $|r_{vv}|^2$. Figure 2(e) shows the intensity $I_{i,j}$ of two anomalous beams, with $i = $ L or R representing LCP or RCP component of the anomalous beam; $j = +1$ or -1 representing, respectively, the anomalous beam $+1$ or -1. Within the wavelength range of 1100–1750 nm, the state of the anomalous beam $+1$ is RCP, and the state of the anomalous beam -1 is LCP. The degree of circular polarization (DOCP) is defined as $|I_{RCP} - I_{LCP}|/|I_{RCP} + I_{LCP}|$, where I_{RCP} and I_{LCP} are the intensity of the RCP and LCP components of the anomalous beam, respectively. The DOCP characterizes the quality of a circularly polarized light. We calculate the DOCP for the beam $+1$, which is larger than 99.5%, as shown in Fig. 2(f). This means that the beam $+1$ is essentially a perfect RCP beam. Similarly, the DOCP of the beam -1 is larger than 99.5% as well, suggesting that the beam -1 is a perfect LCP light.

From Fig. 2(e), one may find that, when the wavelength is shorter than 1100 nm, the light intensity (red and blue lines) is lower than the theoretically expected value $|r_{uv}|^2/2$ (green dashed-dotted line). This effect is due to the coupling of the reflections from different building blocks, which is more evident when the wavelength is comparable to the geometrical size of the building block (600 nm). This effect diminishes greatly when the wavelength becomes much larger than the size of the split ring. The light intensity of the anomalous beam equals $|r_{uv}|^2/2$ in the range 1100–1750 nm.

For the scenario of x-polarized normal incidence, the light reflected by the split ring array can also be treated as the superposition of the rotational component (amplitude of $|r_{uv}|$) and the static component (amplitude of $|r_{vv}|$). In the x-y-z coordinate system, the unit vector of the rotational component $\hat{e}_{rx}$ points to $2\varphi + 90°$, and that of the static component $\hat{e}_{sx}$ points to $0°$. Similar to Eq. (3), the reflected light of the x-polarized incidence $\vec{r}_{ref,x}$ can be expressed as

$$\vec{r}_{ref,x} = r_{vv}\hat{e}_{sx} + r_{uv}\hat{e}_{rx}. \tag{5}$$

For x-polarized incidence, the direction of the rotational component varies at each building block in the unit cell. The angle between the rotational components of the neighboring split rings is $2\Delta\varphi$ (here, $\Delta\varphi$ denotes the difference of the angle rotated by the neighboring rings, $2\Delta\varphi = 45°$ in our case). The spatial arrangement of the rotational component is the same as that shown in Fig. 2(a), so the reflected light under illumination of x- and y-polarized light are the same. Therefore, the RCP anomalous beam propagates in $\vec{k}_{a,+1}$, whereas the LCP anomalous beam propagates in $\vec{k}_{a,-1}$, which is the same scenario as that for the y-polarized incidence.

It should be emphasized that a linearly polarized light can be decomposed into x- and y-polarized components in phase.

The propagation direction and intensity of the RCP (LCP) anomalous beam under both x- and y-polarized incidence are identical. These features do not depend on the polarization direction of the incident light. It follows that, within the response wavelength range, any linearly polarized light (hence, natural light) can be transformed to the anomalous LCP/RCP beams by the metasurface.

It is noteworthy that the phase gradient of the LCP (RCP) anomalous beam is introduced by rotating the unsized split rings, which does not depend on the wavelength of the incident light. Therefore, the advantage of this rotation-induced (in contrast to shape-induced) phase modulation on the metasurface is that the phase gradient is completely independent of the wavelength.

To verify the above calculations, we experimentally fabricate the split ring array on a SiO_2-silver bilayer substrate. First, we deposit a silver layer 100 nm in thickness (h_2) on a cleaned silicon surface by electron beam evaporation. Then on top of the silver layer, a 175 nm thick SiO_2 layer (h_1) is deposited by plasma-enhanced chemical vapor deposition (PECVD). In this way, a SiO_2-silver bilayer is formed. On this bilayer, the silver split ring structure is fabricated with electron beam lithography and liftoff technology as follows. A photoresist stencil layer (200 nm polymethyl methacrylate [PMMA]) is spin-coated on the surface of a SiO_2-silver bilayer substrate. Then electron beam lithography is applied to generate an inverse pattern of split rings with rotating orientations. After development, an array of evacuated split rings is formed on the photoresist layer. In the evacuated region, any deposited metal *et sequentes* will reach the SiO_2 surface to form the desired pattern. A 50 nm thick silver layer is blank deposited over the whole area of the wafer, reaching the surface of the substrate in the evacuated regions and staying on the top of the sacrificial photoresist layer in the other areas. Thereafter, with chemical liftoff technology, the silver-covered region with a photoresist layer underneath is removed, whereas the silver pattern contact with the SiO_2 surface survives. In this way, a split ring array is fabricated on the SiO_2-silver bilayer. The size of the fabricated sample is 1×1 mm. Figure 3(a) shows the scanning electron micrograph of the fabricated array.

A Fourier transform infrared spectrometer (Vertex70v, Bruker) combined with an infrared microscope is used to measure the ordinary reflection beam, which propagates in the $+z$ direction. Figure 3(b) shows the measured spectrum of the light intensity of the ordinary beam, which is in good agreement with the simulation. For the anomalous beam, since its propagation direction varies with wavelength, we build a setup to measure the anomalous beam, as schematically illustrated in Fig. 3(c). The light source is a supercontinuum laser. A monochromer is applied to generate the monochromatic light in the near-infrared frequency [not shown in Fig. 3(c)]. A Glan-Taylor polarizer and an achromatic quarter wave plate are applied to generate the linearly polarized and circularly polarized incident beams, respectively. A CaF_2 lens ($f = 80$ mm, diameter 12.7 mm) focuses the incident light onto the metasurface. The focus light spot is of the order of 0.3 mm, which is much smaller than the size of the fabricated sample (1×1 mm). A germanium photodiode detector is installed on the motorized rotation stage to measure the amplitude of the reflected beam. The polarizer and achromatic quarter wave
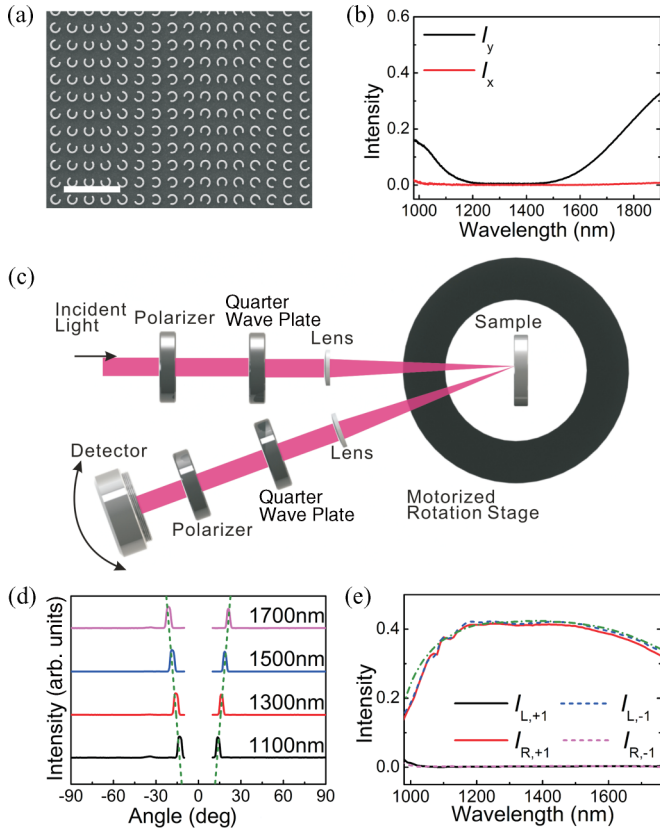
FIG. 3. (Color online) (a) The scanning electron micrograph of the fabricated metasurface. The bar stands for 2 μm. (b) The measured intensity of the x and y components of the ordinary beam. The incidence is y polarized. (c) The schematic diagram of the setup to measure the intensity of anomalous beams. (d) The angle-resolved light intensity distribution for the wavelengths of 1100, 1300, 1500, and 1700 nm, respectively. The green dashed line shows the angle calculated based on Eq. (4). (e) The measured intensity of LCP and RCP components of two anomalous beams. The green dashed-dotted line denotes $|r_{uv}|^2/2$.

plate in front of the detector are used to measure LCP or RCP components of the anomalous beams by tuning the direction of the polarizer. The motorized rotation stage, photodiode detector, and monochromer are all computer controlled. By tuning the monochromer, the incident wavelength can be selected. The direction of the anomalous beam is predicted based on Eq. (3). By rotating the photodiode detector to the direction of the anomalous beam, the intensity of the anomalous beam is measured. The incident beam is set as y polarized. By fixing the wavelength to 1100, 1300, 1500, and 1700 nm, respectively, and continuously rotating the detector stage, we get the angle-resolved light intensity as shown in Fig. 3(d). The green dashed line denotes the predicted reflection direction of the anomalous beam. One may find that the experimental results are in good agreement with the calculation. We change the wavelength of the incident light and measure the intensity of the anomalous beam by rotating the detector. The normalized anomalous beam intensity, which is defined as the ratio of the intensity of the anomalous beam and that of the incidence beam, is illustrated in Fig. 3(e). One may find that the anomalous beam has been effectively generated. Our measurement confirms that

the anomalous beam +1 is RCP and the anomalous beam −1 is LCP, marked by the red and blue lines in Fig. 3(e). The green dashed-dotted line denotes $|r_{uv}|^2/2$. The measurement confirms that the intensity of RCP and LCP equals $|r_{uv}|^2/2$ in the response wavelength range.

This metasurface can also be applied to tune the propagation of circularly polarized light directly. The RCP beam propagating in the $-z$ axis can be expressed as $\frac{\sqrt{2}}{2}(\hat{e}_x + i\hat{e}_y)$. For a split ring with its opening directing to $45° + \varphi$, according to Eqs. (3) and (5), the reflected beam can be expressed as $\frac{\sqrt{2}}{2}r_{vv}(\hat{e}_{sx} + i\hat{e}_{sy}) + \frac{\sqrt{2}}{2}r_{uv}(\hat{e}_{rx} + i\hat{e}_{ry})$, where $\hat{e}_{sx}$ and $\hat{e}_{sy}$ are the unit vectors in the x and y directions; $\hat{e}_{rx}$ and $\hat{e}_{ry}$ are the unit vectors pointing to $2\varphi + 90°$ and 2φ, respectively. It follows that the reflection beam generated by RCP incidence can be expressed as

$$\vec{E}_{\mathrm{ref},R} = r_{vv}\frac{\sqrt{2}}{2}(\hat{e}_x + i\hat{e}_y) + i r_{uv}e^{i2\varphi}\frac{\sqrt{2}}{2}(\hat{e}_x - i\hat{e}_y) \quad (6)$$

where $\frac{\sqrt{2}}{2}(\hat{e}_x + i\hat{e}_y)$ is the unit vector of LCP light and $\frac{\sqrt{2}}{2}(\hat{e}_x - i\hat{e}_y)$ is the unit vector of RCP light propagating along the $+z$ direction. The reflected beam contains both LCP and RCP components. The amplitude of the LCP component is $|r_{vv}|$, and its phase is independent of the orientation of the split ring. The amplitude of the RCP component is $|r_{uv}|$. The phase of the RCP component is 2φ, which is determined by the orientation of the split ring. Therefore, when a RCP incident beam shines on the metasurface, a phase gradient of $\pi/4l$ is established for the RCP component, as we indicated earlier. Consequently, a RCP anomalous beam is generated, and its propagation direction is $\vec{k}_{a,+1}$, as indicated in Fig. 2(c). The amplitude of the RCP component is $|r_{uv}|$, the intensity of RCP anomalous beam equals the polarization conversion ratio $|r_{uv}|^2$. Since the polarization conversion ratio is high (more than 0.8 in the range from 1100 to 1750 nm) in our design, the intensity of the anomalous beam is strong as well. Unlike the reflection from a conventional mirror, which changes an incident RCP to LCP (and vice versa), on this metasurface the anomalous reflection beam keeps the same handedness as that of the incidence beam.

When the incident light is LCP, a similar situation occurs. The phase gradient for the LCP anomalous beam is $-4\pi/l$, and the intensity is $|r_{uv}|^2$. The trajectory of the anomalous beam can be calculated from Eq. (3), and its propagation direction is $\vec{k}_{a,-1}$.

In order to demonstrate that our sample is able to control the propagation direction of the circular polarized light, we change the incidence to RCP/LCP and measure the intensity spectrum of the anomalous beam. Figure 4(a) shows the angle-resolved light intensity distribution at wavelengths 1100, 1300, 1500, and 1700 nm for RCP normal incidence. The green dashed line denotes the direction of the anomalous beam calculated from Eq. (4). One may find that the measured direction of the anomalous beam is in excellent agreement with that predicted by the theory. Figure 4(b) shows the intensity spectrum of the anomalous beam. The black line corresponds to the RCP component, and the red line corresponds to the LCP component. Since the intensity of the LCP component is less than 0.007, and the average intensity of the RCP is higher than 0.7 in the wavelength range 1100–1750 nm, we therefore
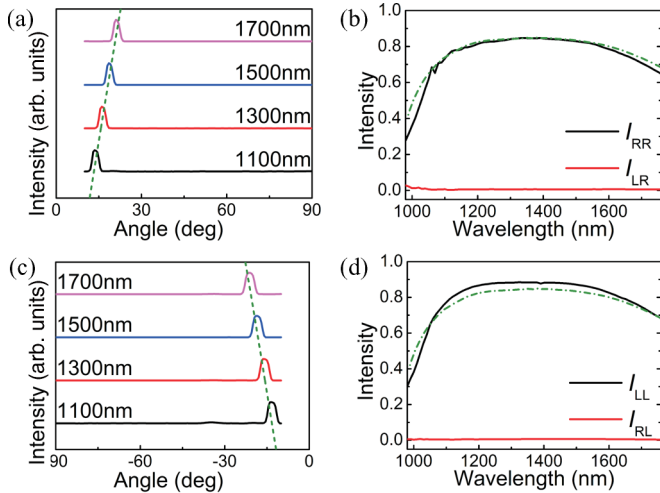
FIG. 4. (Color online) (a) The angle-resolved light intensity of the anomalous beam for RCP incidence. The green dashed line denotes the angle calculated by Eq. (4). (b) The intensity of RCP and LCP components of the anomalous beam for RCP incidence. (c) The angle-resolved light intensity distribution for LCP incidence. The green dashed line denotes the angle calculated by Eq. (4). (d) The RCP and LCP components of the anomalous beam for LCP incidence. The green dashed-dotted lines in (b) and (d) represent $|r_{uv}|^2$.

FIG. 5. (Color online) The plot to show the calculated polarization conversion ratio obtained at different thicknesses of the SiO_2 separation layer as a function of wavelength.

can consider the anomalous beam as a perfect RCP beam. For comparison, the measured polarization conversion ratio $|r_{uv}|^2$, which has been shown in Fig. 1(b), is replotted here with a green dashed-dotted line. One may find that the intensity of the anomalous beam fits $|r_{uv}|^2$ very well.

When the incident beam is LCP, a similar situation occurs. Figure 4(c) illustrates the angle-resolved light intensity for LCP incidence, which indicates that the direction of the anomalous beam fits the theoretical expectation. The measured intensity is demonstrated in Fig. 4(d). The LCP and RCP components are denoted with black and red lines, respectively. Figure 4(d) indicates that the anomalous beam is LCP as well, and the intensity follows the polarization conversion ratio illustrated by the green dashed-dotted line in general. It should be noted that for both RCP and LCP incidence, the measured intensity of the anomalous beam is higher than 0.7 in the range 1100–1750 nm.

The concept of metasurface extends Snell's law to the inhomogeneous interfacial scenario and provides a new degree of freedom in manipulating the propagation of light via controlling the phase gradient on the metasurface [7,8]. By rotating the opening of the split rings, the phase gradient of the circularly polarized light is generated. Since the light intensity of the anomalous beam is directly determined by the polarization conversion ratio, the essential requirement is to design the building block with a large and broadband polarization conversion ratio. As pointed out in Ref. [21], the light reflected by the mirror layer underneath the metasurface can be regarded as the radiation of the mirror image of the metasurface. By tuning the thickness of the dielectric interlayer, the phase difference between the radiation of the metasurface and that from its mirror image can be modulated, and the reflection beam can become dispersion
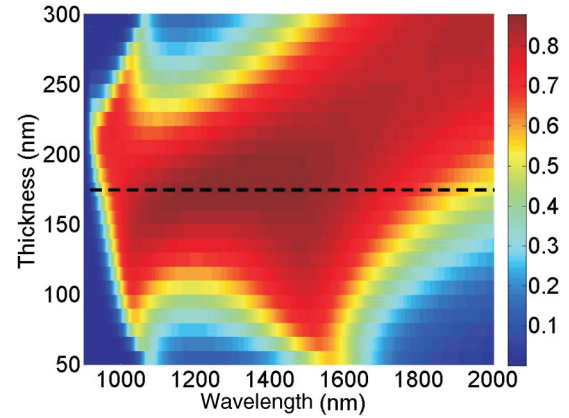
free in a certain wavelength range. With the same geometry, a significantly large polarization conversion ratio can be realized by optimizing the structural geometry and the thickness of the dielectric layer. To illustrate such a relationship, we show in Fig. 5 the polarization conversion ratio obtained at different thicknesses of the SiO_2 separation layer as a function of wavelength. The increment of the SiO_2 layer thickness is 10 nm. The color represents the polarization conversion ratio. One may find that, corresponding to the set of parameters used in the calculation, when the thickness of SiO_2 layer is selected as 175 nm, a flat, large polarization conversion ratio can be realized over a broad wavelength range (the deeper red region marked by the black dashed line). It should be pointed out that a metasurface with a strong anomalous beam intensity and broad bandwidth has been anticipated for many applications. The metasurface reported here converts 80% of incident energy (70% in experiments) to the anomalous beams in the wavelength range 1100–1750 nm. Such a designing strategy is efficient in realizing strong anomalous beams and broad bandwidth simultaneously.

To summarize, we introduce a metasurface made of unsized split rings with rotating opening orientations. The rotating of the split rings generates a phase gradient in the reflection process on the metasurface and contributes to the generation of LCP and RCP beams. Since both rotating split ring and phase conjugation geometry [21] are introduced in our design, a very large polarization conversion ratio and broad bandwidth are simultaneously realized. These features contribute to the high intensity of the anomalous beam over a broad frequency range. We demonstrate that this metasurface can either generate a circularly polarized beam from a linearly polarized or natural light or sort LCP and RCP components of the incidence light to different directions. Practically, the high intensity and broad bandwidth of the anomalous beams can be applied to manipulate the spin state of electrons [1–4] in quantum information technology and to generate vortex beams in vector optics [34,35,41] as well. Furthermore, the principle we applied here in designing the metastructure is universal. We therefore expect that this paper opens a gateway to achieve anomalous beams with better physical features and should be beneficial for the development of nanophotonics.

[1] J. Berezovsky, M. H. Mikkelsen, O. Gywat, N. G. Stoltz, L. A. Coldren, and D. D. Awschalom, Science **314**, 1916 (2006).

[2] M. Kroutvar, Y. Ducommun, D. Heiss, M. Bichler, D. Schuh, G. Abstreiter, and J. J. Finley, Nature **432**, 81 (2004).

[3] K. F. Mak, K. He, J. Shan, and T. F. Heinz, Nat. Nano. **7**, 494 (2012).

[4] J. W. McIver, D. Hsieh, H. Steinberg, P. Jarillo Herrero, and N. Gedik, Nat. Nano. **7**, 96 (2012).

[5] Y. Yang, R. C. da Costa, M. J. Fuchter, and A. J. Campbell, Nat. Photon. **7**, 634 (2013).

[6] M. D. Turner, M. Saba, Q. Zhang, B. P. Cumming, G. E. Schroder-Turk, and M. Gu, Nat. Photon. **7**, 801 (2013).

[7] N. Yu, P. Genevet, M. A. Kats, F. Aieta, J.-P. Tetienne, F. Capasso, and Z. Gaburro, Science **334**, 333 (2011).

[8] A. V. Kildishev, A. Boltasseva, and V. M. Shalaev, Science **339**, 1232009 (2013).

[9] S. Sun, Q. He, S. Xiao, Q. Xu, X. Li, and L. Zhou, Nat. Mater. **11**, 426 (2012).

[10] L. Huang, X. Chen, H. Mühlenbernd, G. Li, B. Bai, Q. Tan, G. Jin, T. Zentgraf, and S. Zhang, Nano Lett. **12**, 5750 (2012).

[11] M. Born and E. Wolf, *Principles of Optics: Electromagnetic Theory of Propagation, Interference and Diffraction of Light* (Cambridge University Press, Cambridge, New York, 1999).

[12] E. Hecht, *Optics* (Addison-Wesley, Reading, MA, 2002).

[13] J. B. Pendry, A. J. Holden, W. J. Stewart, and I. Youngs, Phys. Rev. Lett. **76**, 4773 (1996).

[14] J. B. Pendry, A. J. Holden, D. J. Robbins, and W. J. Stewart, IEEE Trans. Microwave Theory Tech. **47**, 2075 (1999).

[15] N. Fang, H. Lee, C. Sun, and X. Zhang, Science **308**, 534 (2005).

[16] N. I. Landy, S. Sajuyigbe, J. J. Mock, D. R. Smith, and W. J. Padilla, Phys. Rev. Lett. **100**, 207402 (2008).

[17] S.-C. Jiang, X. Xiong, P. Sarriugarte, S.-W. Jiang, X.-B. Yin, Y. Wang, R.-W. Peng, D. Wu, R. Hillenbrand, X. Zhang, and M. Wang, Phys. Rev. B **88**, 161104 (2013).

[18] X. Xiong, W.-H. Sun, Y.-J. Bao, R.-W. Peng, M. Wang, C. Sun, X. Lu, J. Shao, Z.-F. Li, and N.-B. Ming, Phys. Rev. B **80**, 201105(R) (2009).

[19] X. Xiong, W.-H. Sun, Y.-J. Bao, M. Wang, R.-W. Peng, C. Sun, X. Lu, J. Shao, Z.-F. Li, and N.-B. Ming, Phys. Rev. B **81**, 075119 (2010).

[20] X. Xiong, Z. H. Xue, C. Meng, S. C. Jiang, Y. H. Hu, R. W. Peng, and M. Wang, Phys. Rev. B **88**, 115105 (2013).

[21] S.-C. Jiang, X. Xiong, Y.-S. Hu, Y.-H. Hu, G.-B. Ma, R.-W. Peng, C. Sun, and M. Wang, Phys. Rev. X **4**, 021026 (2014).

[22] S. Larouche and D. R. Smith, Opt. Lett. **37**, 2391 (2012).

[23] X. Ni, N. K. Emani, A. V. Kildishev, A. Boltasseva, and V. M. Shalaev, Science **335**, 427 (2012).

[24] F. Aieta, P. Genevet, N. Yu, M. A. Kats, Z. Gaburro, and F. Capasso, Nano Lett. **12**, 1702 (2012).

[25] F. Aieta, P. Genevet, M. A. Kats, N. Yu, R. Blanchard, Z. Gaburro, and F. Capasso, Nano Lett. **12**, 4932 (2012).

[26] S. Sun, K. Y. Yang, C. M. Wang, T. K. Juan, W. T. Chen, C. Y. Liao, Q. He, S. Y. Xiao, W. T. Kung, G. Y. Guo, L. Zhou, and D. P. Tsai, Nano Lett. **12**, 6223 (2012).

[27] A. Pors and S. I. Bozhevolnyi, Opt. Express **21**, 27438 (2013).

[28] A. Pors, M. G. Nielsen, R. L. Eriksen, and S. I. Bozhevolnyi, Nano Lett. **13**, 829 (2013).

[29] W. T. Chen, K.-Y. Yang, C.-M. Wang, Y.-W. Huang, G. Sun, I.-D. Chiang, C. Y. Liao, W.-L. Hsu, H. T. Lin, S. Sun, L. Zhou, A. Q. Liu, and D. P. Tsai, Nano Lett. **14**, 225 (2014).

[30] M. Kang, T. Feng, H.-T. Wang, and J. Li, Opt. Express **20**, 15882 (2012).

[31] X. Yin, Z. Ye, J. Rho, Y. Wang, and X. Zhang, Science **339**, 1405 (2013).

[32] D. Lin, P. Fan, E. Hasman, and M. L. Brongersma, Science **345**, 298 (2014).

[33] N. Yu, F. Aieta, P. Genevet, M. A. Kats, Z. Gaburro, and F. Capasso, Nano Lett. **12**, 6328 (2012).

[34] P. Genevet, N. Yu, F. Aieta, J. Lin, M. A. Kats, R. Blanchard, M. O. Scully, Z. Gaburro, and F. Capasso, Appl. Phys. Lett. **100**, 013101 (2012).

[35] M. Kang, J. Chen, X.-L. Wang, and H.-T. Wang, J. Opt. Soc. Am. B **29**, 572 (2012).

[36] L. Huang, X. Chen, B. Bai, Q. Tan, G. Jin, T. Zentgraf, and S. Zhang, Light. Sci. Appl. **2**, e70 (2013).

[37] C. Pfeiffer and A. Grbic, Phys. Rev. Lett. **110**, 197401 (2013).

[38] F. Monticone, N. M. Estakhri, and A. Alù, Phys. Rev. Lett. **110**, 203903 (2013).

[39] Z. E. Bomzon, V. Kleiner, and E. Hasman, Opt. Lett. **26**, 1424 (2001).

[40] Z. E. Bomzon, G. Biener, V. Kleiner, and E. Hasman, Opt. Lett. **27**, 1141 (2002).

[41] Y. Yang, W. Wang, P. Moitra, I. I. Kravchenko, D. P. Briggs, and J. Valentine, Nano Lett. **14**, 1394 (2014).

[42] H.-T. Chen, J. Zhou, J. F. O'Hara, F. Chen, A. K. Azad, and A. J. Taylor, Phys. Rev. Lett. **105**, 073901 (2010).

[43] N. K. Grady, J. E. Heyes, D. R. Chowdhury, Y. Zeng, M. T. Reiten, A. K. Azad, A. J. Taylor, D. A. R. Dalvit, and H.-T. Chen, Science **340**, 1304 (2013).

[44] A. Pors and S. I. Bozhevolnyi, Opt. Express **21**, 2942 (2013).

[45] Q. Lévesque, M. Makhsiyan, P. Bouchon, F. Pardo, J. Jaeck, N. Bardou, C. Dupuis, R. Haïdar, and J.-L. Pelouard, Appl. Phys. Lett. **104**, 111105 (2014).

[46] A. Pors, O. Albrektsen, I. P. Radko, and S. I. Bozhevolnyi, Sci. Rep. **3**, 2115 (2013).